Wideband Small-Signal Input dq Admittance Modeling of Six-Pulse Diode Rectifiers

Xiaolong Yue, Xiongfei Wang, Frede Blaabjerg
Department of Energy Technology
Aalborg University
Aalborg East, Denmark
yue@et.aau.dk, xwa@et.aau.dk, fbl@et.aau.dk

Dushan Boroyevich, Rolando Burgos, Fred Lee
Center for Power Electronics Systems
Virginia Tech
Blacksburg, USA
dushan@vt.edu, rburgos@vt.edu, fclee@vt.edu

***Abstract*— This paper studies the wideband small-signal input dq admittance of six-pulse diode rectifiers. Considering the frequency coupling introduced by ripple frequency harmonics of d- and q- channel switching function, the proposed model successfully predicts the small-signal input dq admittance of six-pulse diode rectifiers in high frequency regions that existing models fail to explain. Simulation and experimental results verify the accuracy of the proposed model.**

Keywords— six-pulse diode rectifier; wideband modeling; input admittance; high frequency; linear time periodic system

I. INTRODUCTION

Power converters are prone to negative impedance instability due to the constant power control. Modeling of the input dq admittance of three-phase ac systems is an important research topic because the stability of a three-phase power system at an interface can be estimated by the source output impedance and load input admittance [1]-[3].

Because of the high reliability, diode rectifiers are typical solutions for rectifier stages in medium- and high- power applications, including offshore wind power transmission and commercial jet airplanes [4]-[6]. Therefore, the modeling of six-pulse diode rectifiers is important for the design and operation of electrical power systems. Existing modeling methods for six-pulse diode rectifiers can be divided into two groups, one is analytical average modeling methods [7]-[10] and the other is parametric average modeling methods [11]. The first approach derives the model analytically from the state-space equations, describing physical behavior of the diode rectifier. In the second approach, controlled voltage and current sources are used to describe the averaged model, where parameters are obtained numerically from the switching simulation model. However, existing models of six-pulse diode rectifiers fail to give accurate theoretical results for the small-signal input dq admittance [7]-[11]. The analytical averaged value models and parametric averaged value models predict two admittances (Y_{dd} and Y_{qd}) accurately but fail to predict the other two admittances (Y_{dq} and Y_{qq}) beyond switching frequency [12] [13].

This paper studies the small-signal input dq admittance of six-pulse diode rectifiers. The paper shows that existing averaged models give good approximations for the d-channel switching function in both low and high frequency regions but they fail to represent the q-channel switching function when the frequency range of interest is beyond ripple frequency. This conclusion explains the inaccuracy of existing models for Y_{dq} and Y_{qq} at high frequency. Considering the frequency coupling in ac and dc side caused by ripple frequency harmonics of d- and q-channel switching function, this paper proposes a new model and the model successfully predicts the high frequency resonance in the small-signal input dq admittance of six-pulse diode rectifiers that existing models fail to explain.

II. SMALL-SIGNAL INPUT DQ ADMITTANCE OF SIX-PULSE DIODE RECTIFIERS

Fig. 1 shows a six-pulse diode rectifier and Tab. I lists the parameters of the rectifier.

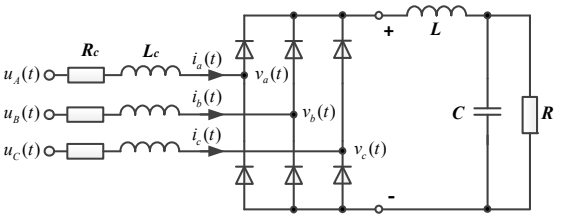

Fig. 1. Six-pulse diode rectifier.

Table I Parameters of the six-pulse diode rectifier.

Description	Parameter values
Voltage source	V_{srms}=120 V, f_s = 60 Hz
AC Inductor	L_c=0.12 mH with ESR 30 mΩ;
DC Inductor	L=2.4 mH with ESR 500 mΩ
DC Capacitor	C=880 μF with ESR 20 mΩ
Load Resistor	R=20 Ω

Fig. 2 gives the simulation and measured results for the input dq admittance of six-pulse diode rectifier [12] [13], in which Y_{dq} and Y_{qq} contain multiple resonant points at high frequency.

A number of averaged models [7]-[11] have been developed to predict the small-signal behavior of six-pulse diode rectifiers. The analytical averaged value models and parametric averaged value models predict two admittances (Y_{dd} and Y_{qd}) accurately but fail to predict the other two admittances (Y_{dq} and Y_{qq}) beyond switching frequency [12] [13].

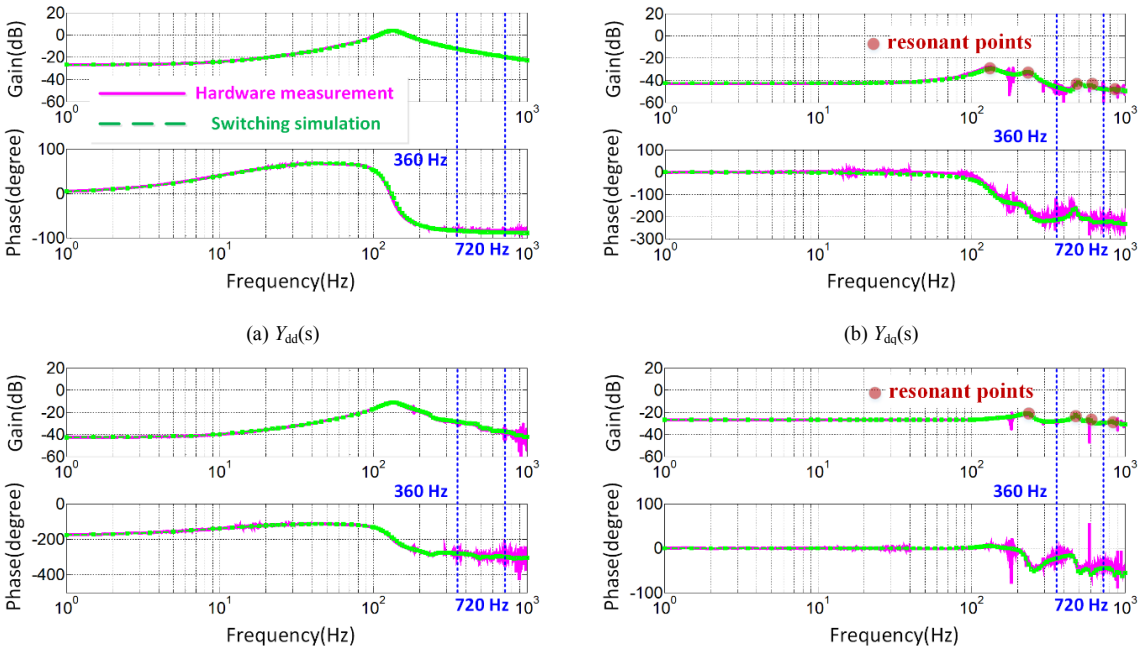

(a) $Y_{dd}(s)$ (b) $Y_{dq}(s)$

(c) $Y_{qd}(s)$ (d) $Y_{qq}(s)$

Fig. 2. Input dq admittance of a six-pulse diode rectifier obtained by switching simulation (green squared line) and hardware measurement (purple straight line). (a) $Y_{dd}(s)$. (b) $Y_{dq}(s)$. (c) $Y_{qd}(s)$. (d) $Y_{qq}(s)$.

III. Proposed Wideband Small-Signal Input dq Admittance Model for Six-Pulse Diode Rectifiers

In Fig.1, the six-pulse diode rectifier can be divided into two parts: an AC side inductor and a six-pulse diode rectifier without AC side inductor. In this section, a six-pulse diode rectifier without AC side inductor will be discussed first and then an AC side inductor will be considered in modeling.

A. D- and Q- Channel Switching Functions of Six-Pulse Diode Rectifier without AC Indcutor

Fig. 3 shows a six-pulse diode rectifier without ac inductor and Fig. 4 gives the switching functions in abc frame when three-phase input voltages are:

$$v_a(t) = V_{in}\sin(2\pi f_s \cdot t)$$

$$v_b(t) = V_{in}\sin(2\pi f_s \cdot t - 2\pi/3)$$

$$v_c(t) = V_{in}\sin(2\pi f_s \cdot t + 2\pi/3)$$

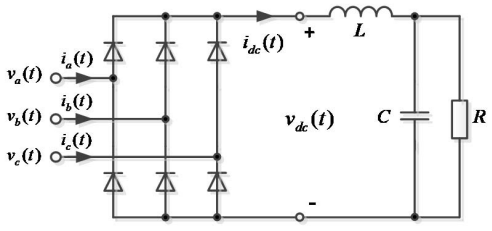

Fig. 3. A six-pulse diode rectifier without an ac inductor.

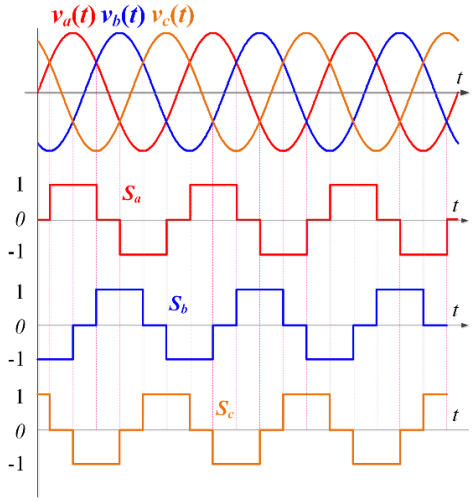

Fig. 4. Switching functions in abc frame.

With the defined switching functions $S_a(t)$, $S_b(t)$ and $S_c(t)$ in abc frame, the current relationship between AC and DC side of the rectifier in Fig. 3 can be expressed as:

$$i_a(t) = i_{dc}(t) \cdot S_a(t)$$

$$i_b(t) = i_{dc}(t) \cdot S_b(t)$$

$$i_c(t) = i_{dc}(t) \cdot S_c(t)$$

and the voltage relationship can be expressed as:

$$v_{dc}(t) = v_a(t) \cdot S_a(t) + v_b(t) \cdot S_b(t) + v_c(t) \cdot S_c(t)$$

With abc/dq transformation

$$T = T_{abc/dq} = \frac{2}{3}\begin{bmatrix} \sin(\omega_0 t) & \sin(\omega_0 t - \frac{2\pi}{3}) & \sin(\omega_0 t + \frac{2\pi}{3}) \\ \cos(\omega_0 t) & \cos(\omega_0 t - \frac{2\pi}{3}) & \cos(\omega_0 t + \frac{2\pi}{3}) \end{bmatrix}$$

where $\omega_0 = 2\pi f_s$ is the grid frequency, d- and q- channel switching functions are defined as:

$$\begin{bmatrix} S_d(t) \\ S_q(t) \end{bmatrix} = T \cdot \begin{bmatrix} S_a(t) \\ S_b(t) \\ S_c(t) \end{bmatrix} \tag{1}$$

and the six-pulse diode rectifier in Fig. 3 can be represented by an equivalent circuit in dq frame, as shown in Fig. 5.

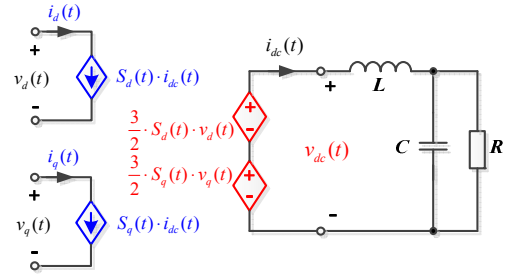

Fig. 5 Equivalent circuit of the six-pulse diode rectifier in dq frame.

According to abc frame switching functions $S_a(t)$, $S_b(t)$ and $S_c(t)$ shown in Fig.4, steady states of d- and q- channel switching functions can be derived as:

$$\begin{aligned} S_{ds}(t) &= \frac{2\sqrt{3}}{\pi} + \sum_{k=0}^{\infty}(-1)^{k+1}\frac{4\sqrt{3}}{(36k^2-1)\pi}\cdot\sin\left[2\pi\cdot 6kf_s\cdot t + \frac{\pi}{2}\right] \\ S_{qs}(t) &= \sum_{k=0}^{\infty}(-1)^{k}\frac{24k\sqrt{3}}{(36k^2-1)\pi}\cdot\sin\left[2\pi\cdot 6kf_s\cdot t\right] \end{aligned} \tag{2}$$

where $k \in Z$ (integer number).

From (2), the steady state of the d- channel switching function S_{ds} is dominated by its dc component, but the steady state of the q- channel switching function S_{qs} only has ripple frequency harmonics ($6kf_s$) and without dc component. In existing models, the averaged values equal to dc components of d- and q- channel switching functions S_{ds} and S_{qs}. Therefore, existing averaged models give good approximations for the d-channel switching function in both low and high frequency regions but they fail to represent the q-channel switching function by its averaged value when the frequency range of interest is beyond ripple frequency ($6kf_s$).

On the other hand, when ripple frequency harmonics of d- and q- channel switching functions are considered in modeling, the six-pulse diode rectifier is a nonlinear time-periodic system with time-periodic operating trajectories, rather than a nonlinear time-invariant system with well-defined dc operating points in dq frame. In traditional small-signal models, the linearization is based on a dc operating point and the linearized model is Linear Time-Invariant (LTI). In contrast, when the linearization is around a time-periodic trajectory, the linearized model is Linear Time-Periodic (LTP).

According to the trajectory linearization [14] and the LTP theory [15], a multiple-input multiple-output model considering the frequency coupling caused by ripple frequency harmonics of d- and q- channel switching functions can be developed, which is similar to the model for single-phase line-frequency rectifiers proposed in [16]. Since the purpose of this paper is to explain high frequency resonance of the measured input dq admittance, following parts of the paper will mainly use equivalent circuits to model and explain the frequency coupling in d- and q- channel, but note that the modeling foundation of this paper is the trajectory linearization and the LTP theory.

B. Modeling for Input DQ Admittance of Six-Pulse Diode Rectifier without AC inductor

Fig. 6 shows a small-signal model for the six-pulse diode rectifier in Fig. 3. The model is expressed by the d- and q-channel switching functions. S_{ds} and S_{qs} are steady state switching functions, $S_{qp}(t)$ represents q- channel switching function's perturbation and I_{dc} is steady state dc current.

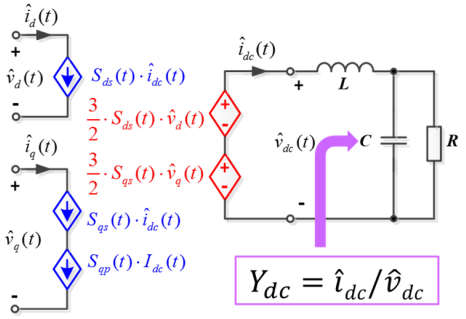

Fig. 6 small-signal model of the six-pulse diode rectifier in dq frame.

By using the method in [16], a model for $S_{qp}(t)$ can be derived similarly as

$$\frac{S_{qp}(f_x + 6kf_s)}{\hat{v}_q(f_x)} = (-1)^k \cdot \frac{3\sqrt{3}}{\pi \cdot V_{in}},\ k = 0, \pm1, \pm2, \cdots \tag{3}$$

where V_{in} is the magnitude of input voltage, f_x is perturbation frequency. The steady state DC current I_{dc} can be calculated as

$$I_{dc}(t) = \frac{2\sqrt{3}}{\pi}\cdot V_{in}\cdot Y_{dc}(0) \tag{4}$$

An input admittance matrix of six-pulse diode rectifiers in dq frame is defined as

$$\begin{bmatrix} \hat{i}_d(t) \\ \hat{i}_q(t) \end{bmatrix} = \begin{bmatrix} Y'_{dd} & Y'_{dq} \\ Y'_{qd} & Y'_{qq} \end{bmatrix} \cdot \begin{bmatrix} \hat{v}_d(t) \\ \hat{v}_q(t) \end{bmatrix} \tag{5}$$

From Fig. 6, the admittances in (5) can be rewritten as

$$\begin{aligned} Y'_{dd} &= \frac{3}{2}\cdot S_{ds}\times Y_{dc}\times S_{ds}, \quad Y'_{dq} = \frac{3}{2}\cdot S_{ds}\times Y_{dc}\times S_{qs} \\ Y'_{qd} &= \frac{3}{2}\cdot S_{qs}\times Y_{dc}\times S_{ds}, \quad Y'_{qq} = \frac{3}{2}\cdot S_{qs}\times Y_{dc}\times S_{qs} + K_{sp} \end{aligned} \tag{6}$$

where $K_{sp} = S_{qp}(t) \cdot I_{dc}(t)$. Fig. 7 shows d- and q- channel equivalent circuit of the six-pulse diode rectifier without AC inductor by using the defined dq admittances in (5) and the d- and q- channel switching functions in (2).

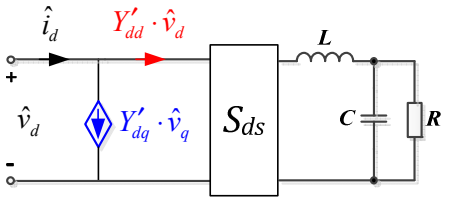

(a) d-channel equivalent circuit

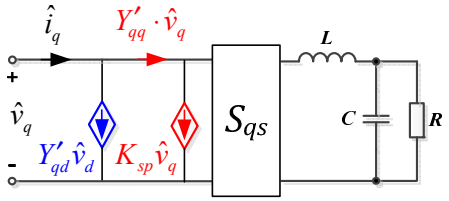

(b) q-channel equivalent circuit

Fig. 7. d- and q- channel equivalent circuits of the diode rectifier in Fig.3.

The d-channel switching function S_{ds} can be approximated by its dc value, so S_{ds} in Fig. 7 (a) can be approximated by a transformer, as shown in Fig. 8.

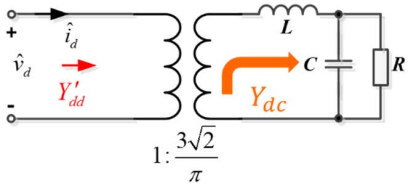

Fig. 8. An equivalent circuit to calculate Y'_{dd}.

From Fig. 8, the admittance Y'_{dd} can be derived as:

$$Y'_{dd}(s) = \frac{18}{\pi^2} \cdot Y_{dc}(s) \tag{7}$$

Fig. 9 shows the frequency characteristics of Y'_{dd}. They have one resonant frequency and its value equals to the resonance frequency of the dc side filter f_R.

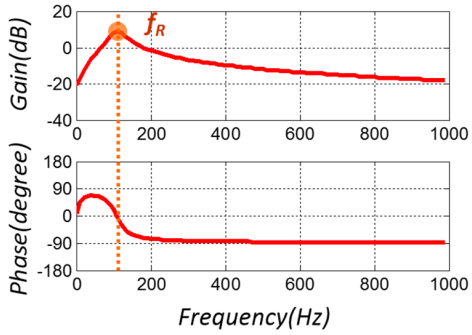

Fig. 9 Frequency characteristics of Y'_{dd}(s).

In contrast, the q-channel switching function has a frequency coupling between left and right side of the switching function. As shown in Fig. 10, a small perturbation $v_q(f_p)$ is modulated by ripple frequency harmonics of the q-channel switching function S_{qs} $(6kf_s)$ and the modulations generate DC voltage components at $f_p \pm 6kf_s$. The DC side circuit is linear so the DC current takes the same frequency components as DC voltage. For those frequency components in DC current, they are modulated by ripple frequency harmonics of the q-channel switching function S_{qs} $(6kf_s)$ and the modulations finally generates $i_q(f_p)$. The frequency coupling in Fig. 10 leads to multiple resonance in the frequency characteristics of Y'_{qq}.

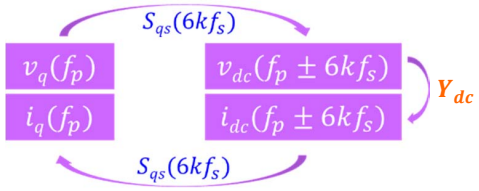

Fig. 10. Frequency coupling analysis for q-channel.

The admittance Y'_{qq} can be derived as:

$$Y'_{qq}(s) = \frac{18}{\pi^2} \cdot Y_{dc}(0) + \sum_{k=0}^{\infty} \frac{648k^2}{\left(36k^2-1\right)^2 \pi^2} \cdot Y_{dc}(s - j2\pi \cdot 6kf_s) - \sum_{k=0}^{\infty} \frac{648k^2}{\left(36k^2-1\right)^2 \pi^2} \cdot Y_{dc}(s + j2\pi \cdot 6kf_s) \tag{8}$$

In (8), the first part represents a constant value, which is given by K_{sp} in (6). The rest of (8) shows the q-channel frequency modulation effect. Fig. 11 shows the frequency characteristics of Y'_{qq}. It has multiple resonances and the resonant frequencies relate to the resonance frequency of the DC side filter f_R and the ripple frequency harmonics $(6kf_s)$.

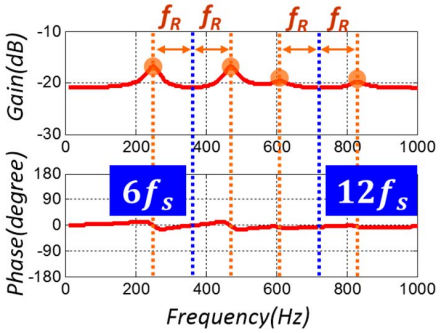

Fig. 11 Frequency characteristics of $Y'_{qq}(s)$.

Admittances Y'_{dq} and Y'_{qd} represent the coupling in d- and q-channel. Fig. 12 shows the frequency coupling analysis for Y'_{dq}.

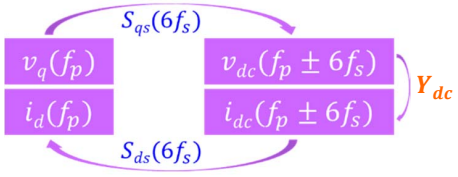

Fig. 12 Frequency coupling analysis for Y'_{dq}.

In Fig. 12, the voltage perturbation $v_q(f_p)$ is first modulated by ripple frequency harmonics of S_{qs} $(6kf_s)$ and then modulated by ripple frequency harmonics of S_{ds} $(6kf_s)$ to generate $i_d(f_p)$. The frequency coupling analysis for Y'_{qd} is similar as that shown in Fig. 12. From Fig. 12, Y'_{dq} and Y'_{qd} can be derived as

$$Y'_{dq}(s) = -Y'_{qd}(s) = \sum_{k=0}^{\infty} \frac{108k}{\left(36k^2-1\right)^2 \pi^2} \cdot e^{j\frac{\pi}{2}} \cdot Y_{dc}(s + j2\pi \cdot 6kf_s) - \sum_{k=0}^{\infty} \frac{108k}{\left(36k^2-1\right)^2 \pi^2} \cdot e^{j\frac{\pi}{2}} \cdot Y_{dc}(s - j2\pi \cdot 6kf_s) \quad (9)$$

Fig. 13 shows the frequency characteristics of Y'_{dq} and $-Y'_{\mathrm{qd}}$. It has multiple resonant points and the resonant frequencies relate to the resonance frequency of the dc side filter f_R and the ripple frequency harmonics. Since the ripple frequency harmonics of the d-channel switching function are small compared with the dc component, the magnitudes of Y'_{dq} and Y'_{qd} are much smaller than the magnitudes of Y'_{dd} and Y'_{qq}.

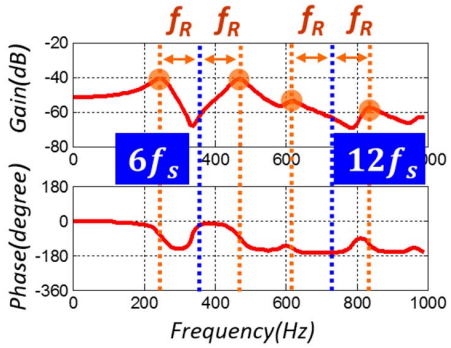

Fig. 13 Frequency characteristics of $Y'_{dq}(s)$ and $-Y'_{qd}(s)$.

However, it should be noted that although d- and q- channel have a weak coupling at perturbation frequency, they take a strong coupling at sidebands. In Fig. 14 (a), when there is a q-channel perturbation $v_q(f_p)$, because the dc component of S_{ds} is much larger than its ripple frequency harmonics, sidebands $i_d(f_p \pm 6kf_s)$ take much larger magnitudes than that of $i_d(f_p)$ in Fig. 12. Similarly, in Fig. 14 (b), when there is a d-channel perturbation $v_d(f_p)$, the magnitudes of sidebands $i_q(f_p \pm 6kf_s)$ are much higher than the magnitudes of the perturbation frequency component $i_q(f_p)$.

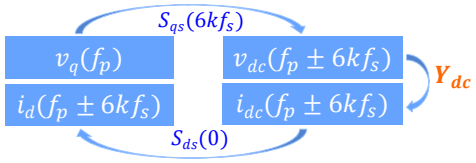

(a) Sideband effect analysis for Y'_{dq}

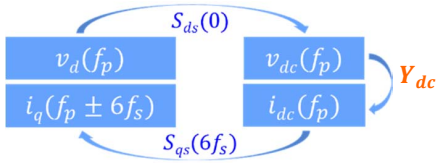

(a) Sideband effect analysis for Y'_{qd}

Fig. 14. Sideband effect in d- and q-channel coupling.

C. *Modeling for Input DQ Admittance of Six-Pulse Diode Rectifier with AC inductor*

In many cases, the AC side inductor in Fig. 1 represents leakage inductance of transformer, which is normally a small value. Since the fundamental voltage in Fig. 1 does not change too much through a small AC inductor, d- and q- channel switching functions can be approximated by S_{ds} and S_{qs} in (1). With this assumption, the six-pulse diode rectifier in Fig. 1 can be represented by the AC inductor in series with the six-pulse diode rectifier without AC inductor.

Fig. 15 shows d- and q- channel equivalent circuits, in which d- and q- channel are coupled through two parts: one is the AC inductor and the other is crossed admittances Y'_{dq} and Y'_{qd}.

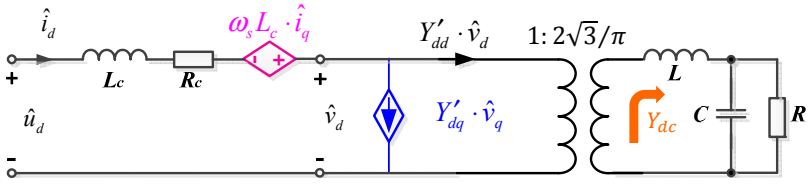

(a) d-channel equivalent circuit

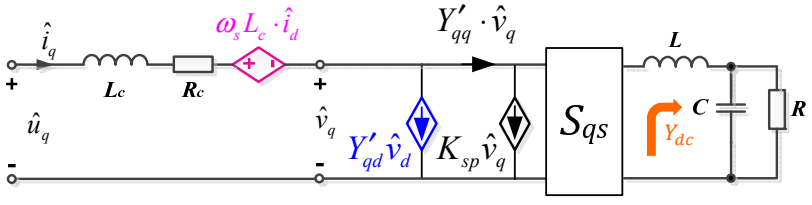

(b) q-channel equivalent circuit

Fig. 15. d- and q- channel equivalent circuits for the six-pulse diode rectifier in Fig.1.

The input admittance matrix for Fig. 15 is defined as

$$\begin{bmatrix}\hat{i}_d(t)\\ \hat{i}_q(t)\end{bmatrix}=\begin{bmatrix}Y_{dd} & Y_{dq}\\ Y_{qd} & Y_{qq}\end{bmatrix}\cdot\begin{bmatrix}\hat{u}_d(t)\\ \hat{u}_q(t)\end{bmatrix} \tag{10}$$

Fig. 16 and Fig. 17 show equivalent circuits to derive Y_{dd} and Y_{qq} respectively, which are obtained by removing coupling items in the d- and q- channel equivalent circuits in Fig. 15.

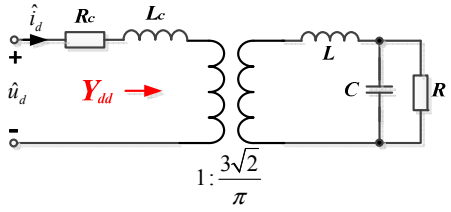

Fig. 16. An equivalent circuit to derive Y_{dd}.

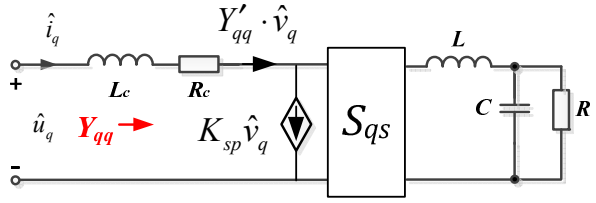

Fig. 17. An equivalent circuit to derive Y_{qq}.

According to the equivalent circuit in Fig. 16, the small-signal input dq admittance Y_{dd} equals to the AC side inductor in series with the admittance Y'_{dd}, so the expression of Y_{dd} is:

$$Y_{dd}(s)\approx\left\{R_c+sL_c+\left[Y'_{dd}(s)\right]^{-1}\right\}^{-1} \tag{11}$$

In Fig. 17, since the AC inductor is assumed to be small, the voltage drop on AC inductor is small and $\hat{v}_q\approx\hat{u}_q$. Thus, the small-signal input dq admittance Y_{qq} approximates to the AC side inductor in series with the admittance Y'_{qq}, which can be expressed as:

$$Y_{qq}(s)\approx\left\{R_c+sL_c+\left[Y'_{qq}(s)\right]^{-1}\right\}^{-1} \tag{12}$$

Fig. 18 and Fig. 19 shows the equivalent circuits to derive crossed admittances Y_{dq} and Y_{qd}. In Fig. 18 and Fig. 19, d- and q- channel are coupled through a voltage source given by the AC side inductor and a current source given by the rectifier without AC inductor. According to Fig. 14, d- and q- channel have strong sideband effects. Since the d-channel is almost linear but the q-channel contains frequency couplings, the sideband effect makes Y_{dq} different from Y_{qd}.

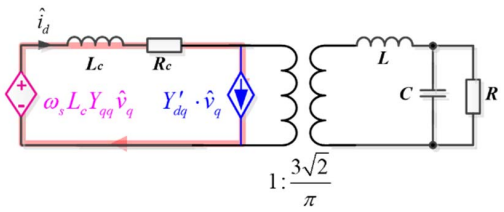

Fig. 18. An equivalent circuit to derive Y_{dq}.

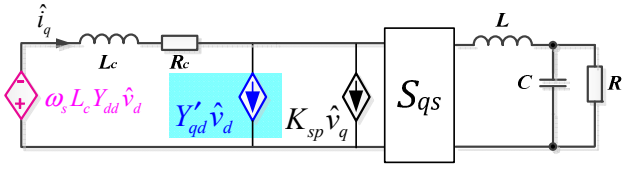

Fig. 19. An equivalent circuits to derive Y_{qd}.

In Fig. 18, the current source $Y'_{\mathrm{dq}}\cdot\hat{v}_q$ contains not only the component at perturbation frequency $i_d(f_p)$, but also multiple sidebands $i_d(f_p\pm 6kf_s)$ with higher magnitudes. Since the d-channel is almost linear and there is no sideband coupling loops, the high magnitude sidebands $i_d(f_p\pm 6kf_s)$ have no effect on the component at perturbation frequency $i_d(f_p)$. From Fig. 18, the small-signal crossed admittance Y_{dq} can be derived by linear circuit theory, which is

$$Y_{dq}(s)\approx\omega_s L_c\cdot Y_{dd}(s)\cdot Y_{qq}(s)+Y'_{dq}(s) \tag{13}$$

In addition, for the current source $Y'_{\mathrm{dq}}\cdot\hat{v}_q$ in Fig. 18, the impedance of its left side circuit is much smaller than the impedance of its right side circuit at high frequency, so current i_d at high frequency approximates to the current source $Y'_{\mathrm{dq}}\cdot\hat{v}_q$. Therefore, the admittance Y_{dq} at high frequency can be further approximated as

$$Y_{dq}(s)\approx Y'_{dq}(s) \tag{14}$$

In Fig. 19, the current source $Y'_{\mathrm{qd}}\cdot\hat{v}_d$ also generates multiple sidebands $i_q(f_p\pm 6kf_s)$. Different from the case in Fig. 18, the q-channel circuit has coupling loops for those sidebands and the component at perturbation frequency. Finally, the admittance Y_{qd} can be derived as:

$$Y_{qd}(s)\approx -Y_{dd}(s)\cdot Y_{qq}(s) \tag{15}$$

Fig. 20 compares the proposed models with switching simulations. To illustrate high frequency resonance more clearly, the figures are presented in a linear scale rather than a log scale. From Fig. 20, the resonant frequencies of Y_{dq}, Y_{qd} and Y_{qq} are related to the resonance frequency of Y_{dd} and ripple frequency harmonics ($6kf_s$). The simulation results verify the accuracy of the proposed model.

In Fig. 20 (b), the mismatch is caused by approximating the d-channel switching function as a transformer and ignoring the sideband coupling in d-channel circuit. However, if the sideband effect in d-channel is considered to derive Y_{dq}, the expression becomes very complex. In this paper, the expression in (13) is selected as a tradeoff between model accuracy and complexity.

When increasing the AC inductance of the six-pulse diode rectifier, the commutation period increases and the error between real switching functions and the expressions in (2) also increases. Then assumptions, such as the voltage drop on AC inductor is small and $\hat{v}_q\approx\hat{u}_q$, are no longer accurate, which will decrease the model accuracy. The large AC inductance case will be studied in future work.

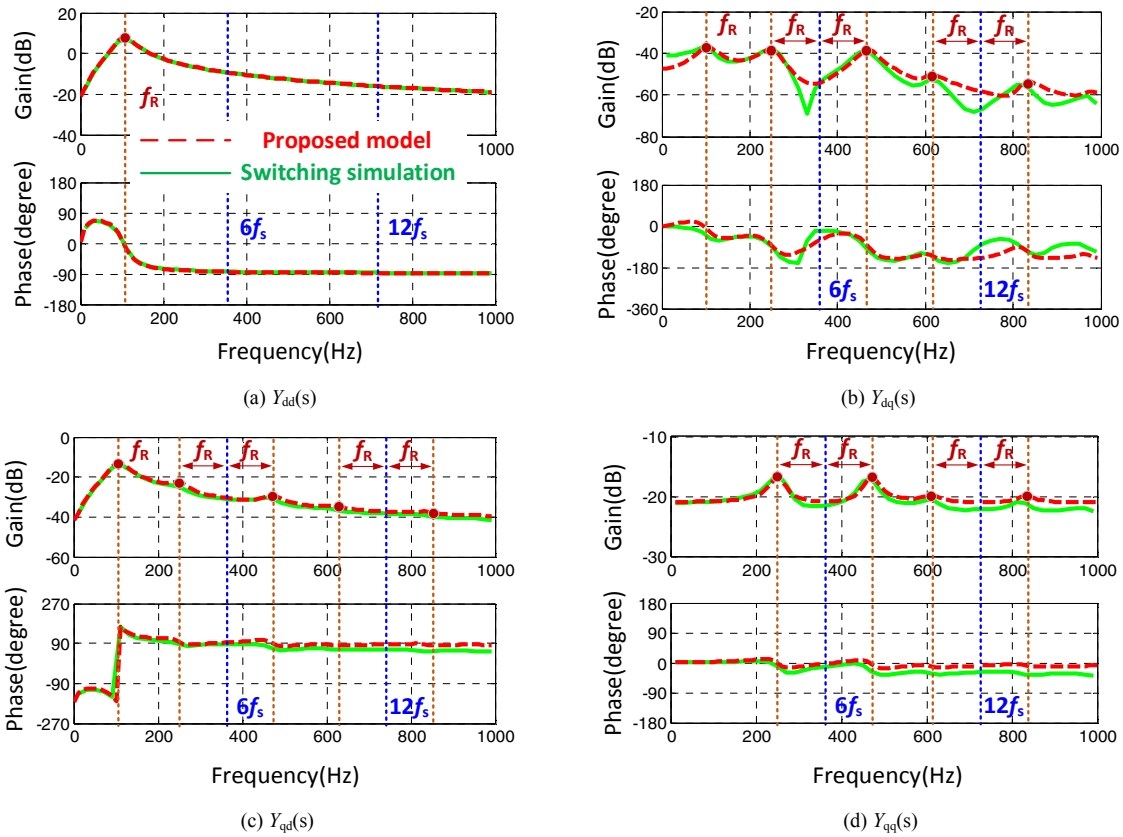

(a) $Y_{dd}(s)$ (b) $Y_{dq}(s)$

(c) $Y_{qd}(s)$ (d) $Y_{qq}(s)$

Fig. 20. Input dq admittance of a six-pulse diode rectifier obtained by switching simulation (green straight line) and the proposed model (red dash line). (a) $Y_{dd}(s)$. (b) $Y_{dq}(s)$. (c) $Y_{qd}(s)$. (d) $Y_{qq}(s)$.

IV. CONCLUSION

This paper studies small-signal input dq admittance of six-pulse diode rectifiers. The d-channel switching function is dominated by its dc value. The q-channel switching function take a zero dc value but it contains large ripple frequency harmonics. From the d- and q-channel switching functions point view, this paper indicates that existing averaged models give good approximations for the d-channel switching function in both low and high frequency regions but they fail to represent the q-channel switching function when the frequency range of interest is beyond ripple frequency. This paper also explains that high frequency resonant points in Y_{dq}, Y_{qd} and Y_{qq} are mainly cased by ripple frequency harmonics of the q-channel switching function. In addition, this paper shows that the admittance Y_{dd} is quite linear, and the admittances Y_{dq} and Y_{qd} are coupled in different ways.

REFERENCES

[1] M. Belkhayat, "Stability criteria for ac power systems with regulated loads," Ph.D. dissertation, Purdue University, Lafayette, IN, 1997.

[2] R. Burgos, D. Boroyevich, F. Wang, K. Karimi, and G. Francis, "On the Ac stability of high power factor three-phase rectifiers," In proc. of Energy Conversion Congress and Exposition (ECCE), 2010 IEEE, 2010, pp. 2047–2054.

[3] X. Wang, F. Blaabjerg and W. Wu, "Modeling and Analysis of Harmonic Stability in an AC Power-Electronics-Based Power System," IEEE Transactions on Power Electronics, vol. 29, no. 12, pp. 6421-6432, 2014.

[4] S. Seman, N. T. Trinh, R. Zurowski, S. Kreplin, "Modelling of the Diode-Rectifier Based HVDC Transmission Solution for Large Offshore Wind Power Plants Grid Access," 15th Wind Integration Workshop, Vienna, Austria, Nov. 2015.

[5] J. Sun and K. J. Karimi, "Small-signal input impedance modeling of line-frequency rectifiers," IEEE Transactions on Aerospace and Electronic Systems, vol. 44, no. 4, pp. 1489-1497, 2008.

[6] Z. Bing, K. J. Karimi and J. Sun, "Input Impedance Modeling and Analysis of Line-Commutated Rectifiers," IEEE Transactions on Power Electronics, vol. 24, no. 10, pp. 2338-2346, 2009.

[7] S. D. Sudhoff and O. Wasynczuk, "Analysis and average-value modeling of line-commutated converter-synchronous machine systems," IEEE Transactions on Energy Conversion, vol. 8, no. 1, pp. 92-99, Mar. 1993.

[8] S. D. Sudhoff, K. A. Corzine, H. J. Hegner, and D. E. Delisle, "Transient and dynamic average-value modeling of synchronous machine fed load-commutated converters," IEEE Transaction on Energy Conversion, vol. 11, no. 3, pp. 508-514, Sep. 1996.

[9] H. Zhu; R. Burgos, F. Lacaux, A. Uan-Zo-li, K.D. Lindner, F. Wang, D. Boroyevich, "Evaluation of average models for nine-phase diode rectifiers with improved AC and DC dynamics," Applied Power Electronics Conf. and Exp., Mar. 2006, pp., 1324-1330.

[10] H. Zhu, "New multi-pulse diode rectifier average models for AC and DC power systems studies," Ph.D. dissertation, Virginia Polytech. Inst. State Univ., Blacksburg, VA, 2005.

[11] J. Jatskevich, S. D. Pekarek, and A. Davoudi, "Parametric averagevalue model of synchronous machine-rectifier systems," IEEE Transaction on Energy Conversion, vol. 21, no. 1, pp. 9-18, Mar. 2006.

[12] M. Jaksic, Z. Shen, I. Cvetkovic, D. Boroyevich, P. Mattavelli, M. Belkhayat, J. Verhulst, " Nonlinear sideband effects in small-signal input dq admittance of six-pulse diode rectifiers," in APEC 2013, pp. 2761-2768.

[13] M. Jaksic, "Identification of Small-Signal dq Impedances of Power Electronics Converters via Single-Phase Wide-Bandwidth Injection," Ph.D. dissertation, Virginia Polytech. Inst. State Univ., Blacksburg, VA, 2014.

[14] A. Packard, K. Poolla and R. Horowitz, "Dynamic Systems and Feedback Class Notes," Department of Mechanical Engineering, University of California Berkeley CA, 2005.

[15] N. M. Wereley, "Analysis and Control of Linear Periodically Time Varying Systems," *Ph. D Dissertation*, Massachusetts Institute of Technology, Boston, 1990.

[16] X. Yue, D. Boroyevich, R. Burgos and F. Zhuo, "Modeling and analysis for input characteristics of line-frequency rectifiers," *2016 IEEE Energy Conversion Congress and Exposition (ECCE)*, Milwaukee, WI, 2016, pp. 1-8